Inter J Nav Archit Oc Engng (2011) 3:159~173
http://dx.doi.org/10.3744/JNAOE.2011.3.3.159

Comparison of potential and viscous methods for the nonlinear ship wave problem

Jin Kim[1], Kwang-Soo Kim[1], Yoo-Chul Kim[1], Suak-Ho Van[1] and Hyo-Chul Kim[2]

[1]*Korea Ocean Research & Development Institute, Daejeon, Korea*
[2]*Department of Naval Architecture and Ocean Engineering, Seoul National University, Seoul, Korea*

ABSTRACT: *The two different numerical approaches for solving the nonlinear ship wave problem are discussed in the present paper. One is based on a panel method, which neglects the viscous effects. The other is based on a finite volume method, which take into account the viscous effects by solving RANS equations. Focus is laid upon on the advantages and disadvantages of two methods. The developed methods are applied to calculating the flow around Series 60 hull to validate the performance of the present nonlinear methods. Although the two methods employ quite different numerical approaches, the calculated wave patterns from both methods show good agreements with the experiments. However the potential method simu-lates the global wave pattern accurately, while the viscous method shows better performance for the local wave prediction near a ship.*

KEY WORDS: Panel method; Finite volume method; Free surface flow; Wave pattern.

INTRODUCTION

The steady ship wave problems have significant importance in marine hydrodynamics. The wave patterns generated by an advancing ship have large influence on the total resistance of a ship. In addition the wave patterns are very sensitive to the details of hull form design and are easily affected by relatively small modifications. Consequently, the capability to predict the wave pattern accurately for a given hull form is an important asset in the initial stage of hull form design. Therefore the effects of a free surface must be taken into account in the relevant methods for solving ship wave problems. The primary difficulties of ship wave problems arise from the nonlinear behavior of the free surface condition, i.e. the boundary condition must be applied on the wavy free surface, which is not known a priori.

The standard approach to the nonlinear ship wave problem may be divided two distinct methods; either the inviscid flow method or viscous flow method. Though the inviscid flow methods don't consider the interaction between the viscous and the wavemaking components, those methods are widely used in marine hydrodynamics because of their robustness and computational efficiency. The inviscid flow methods may be categorized in two general groups, i.e. the panel/boundary element methods (Raven, 1996; Janson, 1997; Kim et al., 1998) and the field methods (Farmer et al., 1994) that solve the Euler equation. The formers have been proven to be the most effective for obtaining fast solutions of nonlinear ship wave problems. At present, panel methods already have reached the maturity for the design tool. And from the numerical point of view, the field methods that solve the discretized Euler equations have inherently the same numerical difficulties of the following viscous flow methods. As a candidate for the inviscid flow calculation the panel/boundary element methods are believed to be better than the field methods with regards to the applicability and computational efficiency of the solution method. Therefore the field methods solving Euler equations are not further considered here.

The viscous flow methods can be divided into two categories based upon the coordinate system in which the governing equations are solved: interface-capturing methods and interface-tracking methods. The interface-capturing methods such as the volume of fluid approach (Schumann, 1998) make use of an inertial coordinate system. In all these approaches a grid fixed in time is used and the free surface is allowed to move between grid points. Thus, tracking the free surface and imposing the boundary conditions on it are not trivial in these approaches. On the other hand, the interface-tracking method, which is also called moving grid approach, makes use of a non-inertial coordinate system and the free surface coincides with a grid surface exactly through the calculations. Thus, imposing the boundary conditions on the free surface as well as tracking the free surface in time is straightforward. However, these approaches involve grid regeneration at every iteration step, which may not be possible for all cases. If the breaking and overturning waves, which are not modeled in panel

Corresponding author: *Jin Kim*
e-mail: *jkim@moeri.re.kr*

methods either, are of no primary interest, the interface-tracking methods are more accurate than the interface-capturing methods with regards to predicting the ship-generated wave patterns. The interface-tracking methods (Muzaferija and Peric, 1997) are therefore adopted in the present work.

Another issue remains for steady nonlinear ship wave problem, i.e. whether a steady-iterative or a time-dependent solution method is to be adopted in the numerical methods for handling the free surface flow. Firstly, the time-dependent solution methods have the advantage with regards to applicability to truly unsteady free surface problems. But it should be pointed out that the steady solution is of primary interest for the nonlinear ship wave problem. From this point of view the discussion will be given below.

For the time-dependent approaches, the simple and natural formulations of the time-stepping procedure are possible. Most time-dependent approaches reach the steady state by starting from the rest and accelerating a ship to its final speed. If the time-dependent solution methods retain the time accuracy in each time steps, much additional flow information besides the steady solution can be obtained. Another advantage of the time-dependent approach is the fact that the initial boundary conditions can be easily given, especially for the viscous methods. This is why most viscous methods for a nonlinear ship wave problem adopt the time-dependent approach.

As opposed to these advantages, the computing demands of relevant methods are significantly excessive before a steady solution is reached. Another difficulty is present in the time-dependent approach, i.e. the non-reflective outer boundary conditions have to be specified. Otherwise the reflective waves will spoil the solution and delay the convergence to a steady state. Some damping zone techniques (Hino, 1994; Hinatsu, 1992), which are adopted in the present viscous method, require the more computing demands due to the additional computational domain for the damping zone.

If the steady solution is of primary interest, steady-iterative solution methods are believed to be more efficient. In the steady-iterative solution methods, the steady solution is found in an iterative procedure starting from the initial guess of the solution. Especially, for the potential methods the good initial guess is available in order to start the iterative procedure. There have been various linear solutions (Raven, 1988) approximating the nonlinear ship wave problem. Following the discussion of Raven (1996), the steady-iterative solution method is adopted for the potential method in the present study.

As mentioned previously, the wave pattern generated by an advancing ship have a dominant effect on the flow around her. In 1994, there has been a workshop (Kodama, 1994) for comparison of the numerical methods that can deal with a free surface flow. In this workshop, Series 60 hull form was used for comparative computations. The numerical results with various potential and viscous methods are collected and compared with the experiments. Recently a number of numerical methods for the nonlinear ship wave problem have been developed and updated since the previous workshop. The present paper is initiated from the questions that how accurately the state-of-the art numerical methods at present can predict the wave pattern generated by a ship and how much the viscosity of the fluid has influence on the stern wave. Therefore the present paper lay a primary emphasis on the capability for predicting the wave patterns around a ship in the potential and viscous methods. The evaluation and validation of both methods will be performed by the detailed comparison at the various longitudinal and transverse cuts with the extensive experimental data by Toda et al. (1991).

The rest of the paper is organized as follows: In section 2, the potential method is described briefly. In section 3, the viscous method with primary emphasis on the numerical method is presented. In section 4, results and discussions are presented and in section 5, conclusions are drawn.

POTENTIAL METHOD

Governing equations and boundary conditions

A right-handed Cartesian coordinate system illustrated in Fig. 1 is used throughout the analysis. The origin is chosen at the intersection of the midship and the still water plane. The x-axis is positive in the downstream direction, the y-axis is positive to the starboard side of a ship and the z-axis is positive up-wards. The incoming free stream is parallel to the x-axis and moves to the downstream direction. In the following equations, all the quantities are nondimensionalized by ship speed U and ship length L and the density of a fluid. As mentioned in section 1, the wave breaking is not regarded in the present approach. Thus the free surface shape will be described as a single-valued function of the horizontal coordinates, $z = h(x, y)$.

In potential flow, it is assumed that the fluid is inviscid and incompressible and the motion is irrotational.

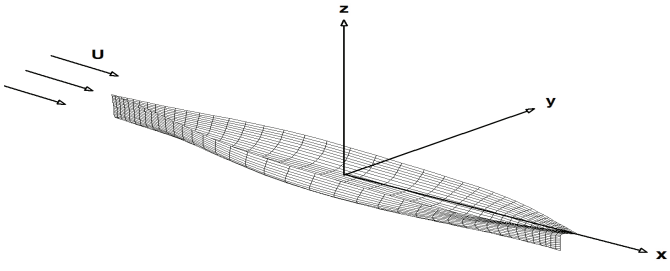

Fig. 1 Coordinate system.

Then the flow can be described by a velocity potential ϕ, which satisfies Laplace equation,

$$\nabla^2 \varphi = 0 . \tag{1}$$

In addition we have the Bernoulli equation the constant C being equal throughout the domain.

$$p + \frac{z}{Fn^2} + \frac{1}{2}\nabla\phi \cdot \nabla\phi = C \tag{2}$$

On the wetted part of the hull a condition of tangential flow is to be satisfied.

$$\phi_n = 0 \tag{3}$$

where n denotes the outward unit normal vector on the hull boundary and the subscript stands for the derivative in that direction.

On the free surface the kinematic condition has the same form of the hull boundary condition.

$$\phi_n = 0 \quad \text{at } z = h(x,y) \tag{4}$$

or, equivalently

$$\phi_x h_x + \phi_y h_y - \phi_z = 0 \quad \text{at } z = h(x,y) \tag{5}$$

The pressure, expressed in the velocities and wave elevation through the Bernoulli equation, must be constant (atmospheric) at the free surface.

$$h = \frac{1}{2} Fn^2 (1 - \varphi_x - \varphi_y - \varphi_z) \quad \text{at } z = h(x,y) \tag{6}$$

where Fn denotes the Froude number($U/\sqrt{gL}$).

Numerical method

Discretization

The raised panel approach is adopted in handling the nonlinear free surface condition. On the hull the familiar distribution of quadrilateral constant-strength source panels is used, with collocation points on the panel centroids. For the free surface panels however, quadrilateral constant-strength source panels are located at a certain distance above the wave surface, while the collocation points are on the wave surface itself (see Fig. 2). As mentioned in Raven (1996) and Janson (1997), this raised panel approach makes the dis-persion and dissipation errors smaller and improves the convergence of the nonlinear iterations.

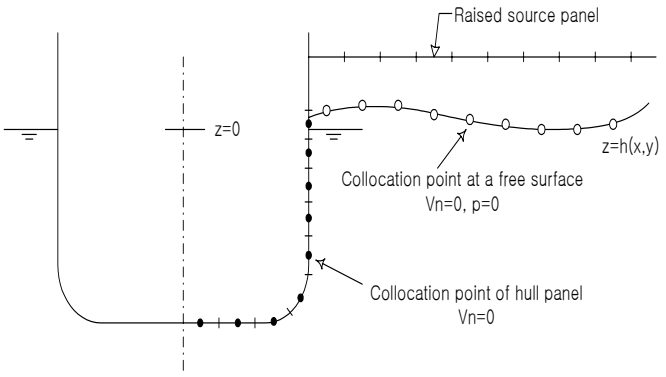

Fig. 2 Schematics of raised panel approach.

The potential ϕ due to the source panels distributed both on the hull surface and on the free surface is

$$\phi(x,y,z) = \sum_{i=1}^{NB+NF} \sigma_i \left(\int_{S_i} \frac{1}{r_{ij}} dS \right) + x \tag{7}$$

where NB and NF are the number of panels on the hull and the free surface, respectively. σ_i is the source density and r_{ij} is the distance from a point on the surface to the field point where the potential is computed. The source panels automatically satisfy the governing equation (1), so their strengths have to be determined from the boundary conditions on the hull (3) and on the free surface (5), (6). The body boundary condition is implemented simply, but the implementation of the free surface conditions deserves some discussion, which will be addressed below.

Nonlinear treatment of a free surface

The present free surface problem is nonlinear since the free surface conditions (5) and (6) are nonlinear and must be satisfied on the initially unknown wave elevation. The solution method for the nonlinear problem described here is to linearize the free surface condition around known base solution Φ and solve the problem in an iterative manner. In each iteration the problem is linearized with respect to the solution from the previous iteration. The first iteration is started from a base flow that may be the undisturbed flow or a zero Froude number flow with a Neumann condition on the free surface. In the first linear solution the linearized free surface conditions are applied on the undisturbed free surface and in the following iterations they are moved to the wavy free surface computed in the previous iteration.

The free surface condition to be imposed in each iteration is derived as follows. The velocity and free surface elevation to be calculated are decomposed as:

$$\nabla\phi = \nabla\Phi + \nabla\phi', \quad h = H + h' \tag{8}$$

where $H(x, y)$ is an assumed wave elevation, $\Phi(x, y, H)$ is a base flow velocity potential on that surface and $\nabla\phi'$, h' are perturbations. The kinematic and dynamic boundary conditions, linearized in these perturbations, then can be written as:

$$\phi_x H_x + \phi_y H_y + \Phi_x h'_x + \Phi_y h'_y - \phi_z = 0 \tag{9}$$

$$h' = \frac{Fn^2}{2}(1 + \Phi_x^2 + \Phi_y^2 + \Phi_z^2 - 2\Phi_x\varphi_x - 2\Phi_y\varphi_y - 2\Phi_z\varphi_z) - H \tag{10}$$

Substituting Equation (10) to Equation (9) results in the combined free surface condition. This combined free surface condition is to be satisfied on the free surface $z = H$.

As can be noticed from Equation (5) and (6), the convergence criteria are the equation residuals in the kinematic and dynamic conditions:

$$\varepsilon_k = \Phi_z - \Phi_x H_x - \Phi_y H_y,$$
$$\varepsilon_d = \frac{Fn^2}{2}(1 - \Phi_x^2 - \Phi_y^2 - \Phi_z^2) - H \tag{11}$$

where $\varepsilon_k < 0.002$ and $\varepsilon_k < 0.0025\ Fn^2$ are used in the present study.

Sometimes if the collocation points are too close to or too far from the free surface panels during the nonlinear iterations, the adaptation of free surface panels according to the collocation points (wave elevation) may be required to maintain the reasonable distance between the collocation points and the wave surface. Particularly, the finer free surface panels require these adaptations. These adaptations of free surface panels, which are not necessary in every iterations, make the dispersion and damping errors to be distributed uniformly.

To enforce the radiation condition, which demands that there are no waves ahead a ship, the present method employs Dawson's 4-point upwind-difference operator (Janson, 1997) in a longitudinal direction. This 4-point upwind-difference operator has less numerical damping than the QUICK scheme of the third order, which is usually used in the viscous methods. For a transverse direction the standard 3-point central-difference operator is employed. Furthermore, collocation points are shifted upstream to smooth out the source strengths and to prevent upstream waves at high speeds. The shifted distance is usually about 25% of the free surface panel length.

The most time-consuming part of solution procedures is solving the resultant linear equation obtained by imposing the boundary conditions. Thus the present method uses the efficient iterative linear equation solver. The adopted preconditioned GMRES is usually 5~7 times faster than the direct method like Gauss elimination. To achieve the convergence of GMRES iterative solver, the linear equation is preconditioned by incomplete Gauss elimination (Söding, 1994). This iterative solver reduces the total calculation time of nonlinear solutions substantially.

Overall solution procedure

The solution algorithm of the potential calculation can be summarized as follows:

1. Choose an initial approximation of the free surface and an initial velocity distribution on that sur-face.
2. In the free surface collocation points, impose a combined free surface condition. Impose the hull boundary condition on the hull collocation points. Solve the resulting set of linear equations for the source strengths.
3. Compute the velocity on the free surface. Calculate a new estimate of the wave elevation from the dynamic free surface condition.
4. Move the free surface collocation points to the new free surface. Adapt the estimated velocity field to the new solution.
5. If necessary, adapt the free surface panels to the new estimated wave surface.
6. Return to step 2 and repeat until the residual errors in Equation (11) are smaller than the specified tol-erances.

VISCOUS METHOD

Governing equations

The governing equations for turbulent flow in the present study are Reynolds-averaged Navier-Stokes equations for momentum transport and continuity equation for mass conservation.

$$\frac{\partial u_k}{\partial x_k} = 0 \tag{12}$$

$$\frac{\partial u_i}{\partial t} + \frac{\partial [u_i (u_j - u_{bj})]}{\partial x_j} = -\frac{\partial \hat{p}}{\partial x_i} + \frac{\partial \tau_{ij}}{\partial x_j} + b_i \tag{13}$$

Where $u_i=(u, v, w)$ are the velocity components in $x_i=(x, y, z)$ directions, u_{bi} is the velocity of the moving grid, $\hat{p}$ is the modified pressure, τ_{ij} is the component of the viscous stress tensor, b_i is the body force in the direction of the Cartesian coordinate x_i.

The present viscous method reaches the steady state by starting from the rest and accelerating a ship to its final speed. For that purpose the body force in Equation (13) is included, which makes the constant acceleration until the inflow velocity becomes the prescribed value. The modified pressure in Equation (13) is defined as follows:

$$\hat{p} = p - \frac{-z}{Fn^2} + \frac{2}{3}k \tag{14}$$

where p is the original pressure, Fn is the Froude number ($U/\sqrt{gL}$) and k is the turbulent kinetic energy. It should be noted that the modified pressure includes the hydrostatic pressure term ($-z/Fn^2$) for the gravitational force because the present viscous method takes into account the effects of the free surface.

In interface-tracking methods similar to the present method, the grid is fitted to the free surface and follows its movement, which requires the use of a moving grid. As shown in Equation (13), the convection term thus includes the velocity of the moving grid. Also, the so-called space conservation law has to be satisfied for the velocity of a moving grid. This discussion will be addressed in the following subsection. The viscous stress tensor can be written using Boussinesq's isotropic eddy viscosity hypothesis as follows:

$$\tau_{ij} = (\frac{1}{\mathrm{Re}} + \nu_t)(\frac{\partial u_i}{\partial x_j} + \frac{\partial u_j}{\partial x_i}) = \nu_e(\frac{\partial u_i}{\partial x_j} + \frac{\partial u_j}{\partial x_i}) \tag{15}$$

where Re is the Reynolds number (UL/ν), ν_t is the turbulent eddy viscosity and ν_e is the effective eddy viscosity. It is noted that the term with turbulent kinetic energy is included in the pressure term as shown in Equation (14). For turbulence closure, the standard k-ε model is utilized. With the k-ε two-equation turbulence model, the eddy viscosity can be written as

$$\nu_t = C_\mu \frac{k^2}{\varepsilon} \tag{16}$$

k and ε are obtained from the solutions of their modeled transport equations, which can be written in a general form as:

$$\frac{\partial \varphi}{\partial t} + \nabla \cdot (\boldsymbol{v}\varphi) = \nabla \cdot \left[\left(\nu + \frac{\nu_t}{\sigma_\varphi} \right) \nabla \varphi \right] + S_\varphi \tag{17}$$

where $\varphi = k, \varepsilon$. For the standard k-ε model, the source terms in Equation (17) are:

$$S_k = P_k - \varepsilon$$

$$S_\varepsilon = C_{\varepsilon 1} \frac{\varepsilon}{k} P_k - C_{\varepsilon 2} \frac{\varepsilon^2}{k} \tag{18}$$

$$P_k = \nu_t \left(\frac{\partial u_i}{\partial x_j} + \frac{\partial u_j}{\partial x_i} \right) \frac{\partial u_i}{\partial x_j}$$

The model constants are given by:

$$C_\mu = 0.09,\ C_{\varepsilon 1} = 1.44,\ C_{\varepsilon 2} = 1.92,\ \sigma_k = 1.0,\ \sigma_\varepsilon = 1.3 \tag{19}$$

For the economy and robustness of the present viscous method, the so-called Launder and Spalding's wall function is utilized to bridge the fully turbulent region and the wall.

Numerical method

Discretization

The cell-centered finite volume method is utilized to discretize the governing equations, as discussed in Ferziger and Peric (1996), Kim (1999). The governing equations are integrated over cell volume Ω with boundary surface S, resulting in the following equations.

$$\int_S \boldsymbol{v} \cdot \boldsymbol{n} dS = 0 \tag{20}$$

$$\begin{aligned} &\frac{\partial}{\partial t} \int_\Omega u_i d\Omega + \int_S u_i (\mathbf{v} - \mathbf{v}_b) \cdot \mathbf{n} dS \\ &\quad = \int_S \tau_{ij} \mathbf{i}_j \cdot \mathbf{n} dS - \int_S \hat{p} \mathbf{i}_i \cdot \mathbf{n} dS + \int_\Omega b_i d\Omega \end{aligned} \tag{21}$$

where $\boldsymbol{v}$ is the fluid velocity vector whose Cartesian components are $\boldsymbol{u}_i$, $\boldsymbol{v}_b$ is the velocity of the surface S, τ_{ij} is the components of the viscous stress tensor, $\boldsymbol{i}_j$ is the unit vector in x_j direction, $\hat{p}$ is the modified pressure, b_i is the body force in the direction of the Cartesian coordinate x_i, and $\mathbf{n}$ is the unit normal vector on the surface S pointing outward.

The unsteady term in the momentum transport equation is approximated by implicit Euler scheme, since only the steady solution is of the present interest. The convection term in Equation (13) is nonlinear and linearization is necessary for simplicity. The widely used approach is that the mass flux through the cell face is taken from the previous iteration. The convective flux of u_i through the face of the surface S_c is then discretized using QUICK scheme of the third order as follows:

$$F_{i,c} = \int_{Sc} u_i (\boldsymbol{v} - \boldsymbol{v}_b) \cdot \boldsymbol{n} dS \approx \dot{m}_c u_{i,c}^{QUICK} \tag{22}$$

where $\dot{m}_c$ is the mass flux through the face of the surface S_c. The QUICK scheme requires 13-point stencil, resulting in complicated algebraic equations. Thus, the so-called deferred correction approach (Khosla and Rubin, 1974) is adopted, which a simple upwind difference scheme (UDS) is used with lagged higher order terms. The deferred correction makes 7-point stencil with simple linear equations.

$$F_c = F_c^{UDS} + (F_c^{QUICK} - F_c^{UDS})^{old} \tag{23}$$

The term in parenthesis (denoted by the superscript "old") is calculated explicitly using the value at the preceding outer iteration level and treated as a known value.

The mass flux in Equation (22) is discretized using the midpoint rule as follows:

$$\dot{m}_c = \int_{S_c} (\boldsymbol{v} - \boldsymbol{v}_b) \cdot \boldsymbol{n} dS \approx (\boldsymbol{v} \cdot \boldsymbol{n})_c S_c - \dot{\Omega}_c \tag{24}$$

The volume flux $\dot{\Omega}_c$ in Equation (24) is calculated from the so-called space conservation law, which is expressed as:

$$\frac{d\Omega}{dt} - \int_S \boldsymbol{v}_b \cdot \boldsymbol{n} dS = 0 \tag{25}$$

when the control volume moves, the above relation between the rate of change of control volume and its surface velocity has to be satisfied. Otherwise, artificial mass sources are introduced and accumulated, and they may spoil the solution.

The conservation equation for space can be discretized using the implicit Euler scheme as follows:

$$\frac{\Omega^{n+1}-\Omega^{n}}{\Delta t}=\sum_{c}(\boldsymbol{v}_b\cdot\boldsymbol{n})_c S_c \tag{26}$$

where the superscripts n+1 and n indicate the new and old time levels, respectively. The volume change of the left-hand term in Equation (26) can be expressed through the sum of the volume $\delta\Omega_c$ swept by the control volume faces during the time Δt:

$$\Omega^{n+1}-\Omega^{n}=\sum_{c}\delta\Omega_c \tag{27}$$

The volume flux caused by the movement of the control volume face can therefore be expressed as follows:

$$\dot{\Omega}_c=(\boldsymbol{v}_b\cdot\boldsymbol{n})_c S_c=\frac{\delta\Omega_c}{\Delta t} \tag{28}$$

Rewriting the viscous stress tensor of Equation (21) gives

$$\begin{aligned}\int_S \tau_{ij}\mathbf{i}\cdot\mathbf{n}dS&=\int_S \nu_e\left(\frac{\partial u_i}{\partial x_j}+\frac{\partial u_j}{\partial x_i}\right)\mathbf{i}_j\cdot\mathbf{n}dS\\&=\int_S \nu_e\left(\nabla u_i\cdot\mathbf{n}+\frac{\partial u_j}{\partial x_i}\mathbf{i}_j\cdot\mathbf{n}\right)ds\end{aligned} \tag{29}$$

The central difference scheme (CDS) is utilized for diffusion terms, while the terms coming from grid non-orthogonality is deferred. Finally, the pressure term and the body force term in the momentum transport equation are discretized by the midpoint rule.

The resulting algebraic approximations of the governing equations are obtained for each control volume in the following form:

$$A_P\varphi_P+\sum_l A_l\varphi_l=Q_p \text{ where } l=E,W,N,S,T,B \tag{30}$$

where φ stands for a general dependent variables, A_P is the coefficient of the cell-centered node P, A_l are the coefficients that multiply the values of φ at centers of neighbor cells and Q_P contains source terms and contributions from convective and diffusive fluxes. The above linear equations obtained from 7-point stencil are solved using strongly implicit procedure (Stone, 1968).

If the pressure field is known a prior, momentum equations will give correct velocity field. However, those velocity components will not satisfy the continuity equation. To ensure divergence-free velocity field, the SIMPLE method is employed. Since the collocated grid arrangement is chosen, the artificial dissipation term in pressure correction equation is added, as discussed in Rhie and Chow (1983). As mentioned in the above momentum equation, pressure correction equation also have the terms related to grid skewness. In the present study, as recommended in Ferziger and Peric (1996), the second correction is added to compensate for deferred correction terms in pressure correction equation. Again, the resulting linear equations are solved using strongly implicit procedure until the equation residual drops by an order of magnitude each iteration.

Nonlinear treatment of a free surface and other boundary conditions

As mentioned previously in the potential method, there are two boundary conditions to be satisfied on a free surface, i.e., the kinematic and dynamic free surface conditions. The kinematic free surface condition in the viscous method is also expressed as the same form of the potential method, which implies that the normal velocity or mass flux on a free surface is zero. On the other hand the dynamic free surface condition in the viscous method has somewhat different form due to the viscous stresses and the surface tension. But we are not willing to resolve the thin boundary layer near a free surface, the viscous stresses and the surface tension are neglected in this study. The dynamic free surface condition then reduces to the statement that the pressures is zero on a free surface. Consequently, the two free surface conditions have the same form in potential and viscous methods. The kinematic and dynamic free surface conditions in the present viscous method are expressed as follows:

- Kinematic free surface condition

$$\left[(\boldsymbol{v}-\boldsymbol{v}_b)\cdot\boldsymbol{n}\right]_{fs}=0 \quad \text{or} \quad \dot{m}_{fs}=0 \quad at\ z=h(x,y) \tag{31}$$

- Dynamic free surface condition

$$p_{fs}=0 \quad \text{or} \quad \hat{p}_{fs}=\frac{h}{Fn^2} \quad at\ z=h(x,y) \tag{32}$$

where "*fs*" denotes a free surface and h is wave elevation.

The predictor-corrector scheme inherent to all SIMPLE-type methods is used to force the satisfaction of both the kinematic and dynamic conditions at the free surface boundary. The implementation of the dynamic free surface condition is rather simple when the inviscid form is used in the present viscous method. The dynamic condition is included in the solution of momentum equations by treating the free surface as a boundary with the prescribed pressure. With this approach, at the end of a SIMPLE step, the dynamic condition is satisfied, but the kinematic one is not satisfied.

The kinematic condition and the space conservation law are used to control the movement of the free surface. The mass flux through the free surface in discrete form is given by

$$\dot{m}_{fs}=\int_{fs}(\boldsymbol{v}-\boldsymbol{v})_{fs}\cdot\boldsymbol{n}dS\approx(\boldsymbol{v}\cdot\boldsymbol{n}S)_{fs}^{n+1}-\dot{\Omega}_{fs} \tag{33}$$

where the superscript n+1 denotes the next time level. $\dot{\Omega}_{fs}$ is the volume flux swept by the free surface cell face over the time step. The expression for the fluid velocity at the free surface $\boldsymbol{v}_{fs}$ is obtained using the case of prescribed pressure boundaries (Ferziger and Peric, 1996), leading to the following expression:

$$\boldsymbol{v}_{fs} = \bar{\boldsymbol{v}}_{fs} + \frac{\Omega_P}{A_P}\left[\frac{(\nabla p)_P \cdot \boldsymbol{d}_{fs}}{\left|\boldsymbol{d}_{fs}\right|} - \frac{p_{fs} - p_P}{\left|\boldsymbol{d}_{fs}\right|}\right]\frac{\boldsymbol{d}_{fs}}{\left|\boldsymbol{d}_{fs}\right|} \tag{34}$$

where the subscript fs denotes the center of the free-surface control volume face, P denotes the cell center, Ω_p is the volume of the cell, A_p is the central coefficient of the momentum equation, $\boldsymbol{d}_{fs}$ is the relative position vector of the free-surface cell-face center with respect to the cell center P, and the overbar denotes extrapolated value. The simple zero-gradient extrapolation is used here to calculate $\bar{\boldsymbol{v}}_{fs}$, that is, $\bar{\boldsymbol{v}}_{fs} = \boldsymbol{v}_P$.

The cell-face velocities obtained from Equation (34) are corrected upon solving the pressure-correction equation by the amount of:

$$\boldsymbol{v}'_{fs} = -\frac{\Omega_P}{A_P}\left(\frac{p'_{fs} - p'_P}{\left|\boldsymbol{d}_{fs}\right|}\right)\frac{\boldsymbol{d}_{fs}}{\left|\boldsymbol{d}_{fs}\right|} \tag{35}$$

The above cell-face velocities with the correction lead to nonzero mass fluxes $\dot{m}_{fs}$ through the free surface (note that $p'_{fs} = 0$ since the pressure is prescribed at the free surface). In order to satisfy the kinematic free surface condition, the vertices that define the boundary cell face have to be moved, such that the correction of the volume swept by the free surface $\dot{\Omega}'_{fs}$ compensates the mass flux obtained in the preceding step:

$$\dot{m}_{fs} + \dot{\Omega}'_{fs} = 0 \tag{36}$$

Implementing Equation (36) for the free surface movement is very essential problem for the efficiency and stability of the method and there can be many possibilities. Here we adopt the method by Muzaferija and Peric (1997), which uses the iterative correction approach. Furthermore we adopt the so-called background grid in order to reduce the efforts for reconstructing the field grid fitted to the free surface. The purpose of the background grid is to provide predetermined girthwise grid paths along which not only the free surface grid points are allowed to move, but also the actual computational grid points are generated by the interpolation. As shown in Fig. 3, the background grid is constructed to cover the domain above the still water surface for the allowance of maximum wave elevation.

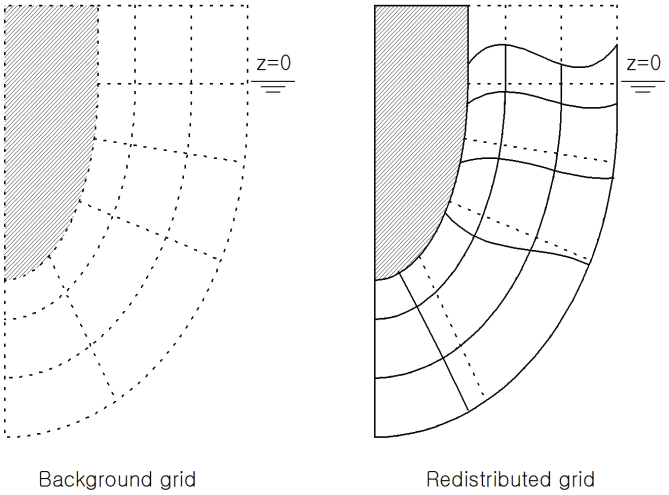

Fig. 3 Redistribution of grids using the background grid.

The first estimate of the free surface movement is obtained by assuming that the correction of volume flux $\dot{\Omega}'_{fs}$ results from displacing of the boundary cell face S_{fs} by Δh in the direction of a unit vector $\boldsymbol{e}^c_{fs}$. The displacement Δh from this approximation is

$$\Delta h = \alpha_{fs}\frac{-\dot{m}_{fs}}{\boldsymbol{S}_{fs} \cdot \boldsymbol{e}^c_{fs}}\Delta t - W(x,y)\,h\,\Delta t \tag{37}$$

where $0 < \alpha_{fs} \leq 1$ is an under-relaxation factor, the vector $\boldsymbol{e}^c_{fs}$ is a unit vector at the cell face center taken as the direction of the grid line of the background grid and h is the wave elevation at the preceding outer iteration. The last term of RHS in Equation (37) is the damping term to avoid the reflection of waves, which will be discussed below. When the outer iterations for one time step converge, the height correction Δh will become negligible since $\dot{m}_{fs}$ goes to zero.

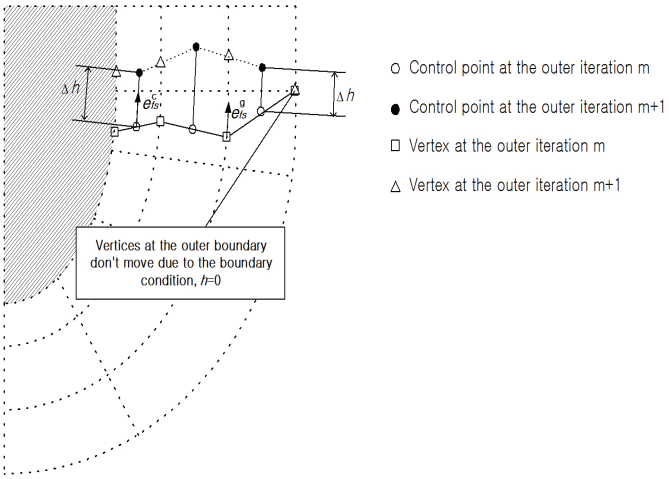

Fig. 4 Procedure of the free surface movement in the viscous method.

As mentioned in Muzaferija and Peric (1997), the free surface control points are introduced for each boundary cell face that coincides with the free surface (see Fig. 4). Their position is controlled by the displacements Δh calculated from Equation (37), while they control the movement of the vertices that define the free surface boundary cell faces.

The position vectors of the free surface control points $\boldsymbol{r}_c$ are adjusted according to the expression

$$\boldsymbol{r}_c^{m+1} = \boldsymbol{r}_c^{m} + \Delta h\, \boldsymbol{e}_{fs}^{c} \tag{38}$$

where m is the counter of the outer iterations within the one time step. The next step is to reconstruct the free surface by modifying the position vectors of vertices $\boldsymbol{r}_v$ that define the free surface boundary, according to the expression:

$$\boldsymbol{r}_v^{m+1} = \boldsymbol{r}_v^{m} + \boldsymbol{e}_{fs}^{g} \cdot \Big(\sum_{i=1}^{N_c} c_i \boldsymbol{r}_{c,i}^{m+1} - \boldsymbol{r}_v^{m}\Big)\, \boldsymbol{e}_{fs}^{g} \tag{39}$$

where N_c is the number of free surface boundary cell faces that share a vertex, c_i is a interpolation factor and $\boldsymbol{e}_{fs}^{g}$ is a unit vector at a vertex. In this study, the bilinear interpolation is used to calculate the increment Δh (the first term in the parenthesis) at a vertex.

Once wave heights at the vertices at the free surface are obtained as a solution of Equation (39), the free surface grid is moved along $\boldsymbol{e}_{fs}^{g}$ vector to the location of the position vector $\boldsymbol{r}_v^{m+1}$ and then projected to the background grid to preserve the smoothness. The grid points below the free surface are then redistributed by the three-dimensional parametric cubic spline using the arc-length distribution of the computational grid at the previous outer iteration level.

Since a cell-centered finite volume approach is used, the boundary values of the flow variables at the free surface are stored at the centers of the cell faces. However, the motion of the free surface is tracked by applying Equation (39) at the cell vertices. This calls for interpolation of the wave heights and geometry-related variables (e.g. unit vectors along the background grid), which introduces noise (short wave oscillations) in the computed wave profiles. The numerical filter reported by Miyata et al. (1987) and Beddhu et al. (1998) is found quite useful to remove these short wave oscillations so as to get a smooth wave profile.

Other boundary conditions

The damping function $W(x, y)$ in Equation (37) deserves some considerations. At the beginning of stage in the present time-dependent approach the waves with all lengths can be generated, including those moving faster than the ship itself. Such waves must be allowed to leave the computational domain through the outer boundaries without too much reflection. Otherwise they will spoil the solution and delay the convergence to a steady state. But, in particular for three-dimensional nonlinear wave problems, the satisfactory and efficient non-reflective boundary conditions are not yet available. As a possible candidate, Hino (1994) showed the effective wave damping technique in his simulation of the similar nonlinear ship wave problem. Following the Hino's approach, the damping term is added to the kinematic free surface condition to reduce the amplitude of waves approaching to outer boundaries. The used damping function $W(x, y)$ is defined as:

$$\begin{aligned} &W(x,y) = A \times \max(W^x(x), W^y(y)) \\ &W^x(x) = \begin{cases} \left(\dfrac{x - x_d}{x_o - x_d}\right)^2 & if\ x_d \le x \le x_o \\ 0 & otherwise \end{cases} \\ &W^y(y) = \begin{cases} \left(\dfrac{y - y_d}{y_o - y_d}\right)^2 & if\ y_d \le y \le y_o \\ 0 & otherwise \end{cases} \\ &0 \le A \le 1/\Delta t \end{aligned} \tag{40}$$

where x_d, y_d is the coordinate from which the damping region starts and x_o, y_o is the location of outflow boundary and outer boundary, respectively. A is the parameter that controls the amount of damping.

Besides the above free surface conditions, the numerical treatments on other boundary conditions (e.g. body surface, inflow plane, outflow plane, outer plane, symmetry plane) are described in Ferziger and Peric (1996). It should be noted that the outflow and outer boundary conditions for wave height is zero because of using the damping function.

Overall solution procedure

The solution algorithm of the viscous calculation can be summarized as follows:

The initial condition is the still state, i.e., velocity, modified pressure and wave height is zero everywhere. The constant acceleration is made in the initial time steps until the inflow velocity becomes the prescribed value (u=1). The following procedures in each time step are continued until the steady state is reached.

1. Solve the momentum equations with the free surface defined previously and the prescribed pressure on it.
2. Enforce local mass conservation in each control volume by solving the pressure-correction equation, using the prescribed pressure boundary condition on the present free surface.
3. Solve the turbulence equations and update the eddy viscosity.
4. Update the position of the free surface to enforce the nonzero mass flux through the free surface based on Equation (39) and regenerate the field grid fitted to the new free surface.
5. Return to step 1 and repeat computation until all equations and boundary conditions are satisfied.
6. Advance to the next time step.

RESULTS & DISCUSSIONS

Computational conditions

The validation calculations are performed for a Series 60 (Cb=0.6) hull in fixed condition. For this case a very extensive set of measurements is available. Especially, a large number of longitudinal and transverse cuts have been measured in the experiments. Following the measurement conditions by Toda et al. (1991), the Froude number is set to 0.316 both in potential method and in viscous method. Additionally, for the viscous method the Reynolds number is set to 4×10^6. Fig. 5 provides the overall picture of the free surface panels for the potential method and the free surface grids for the viscous method. It can be noticed clearly that the viscous method requires more free surface grids than the potential method, which is partly due to the damping zone used in the viscous method.

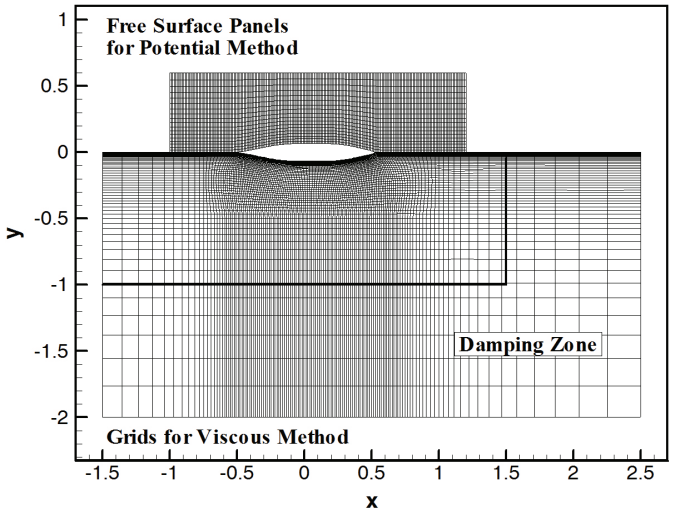

Fig. 5 Free surface panels of potential method and free surface grids of viscous method.

Potential method (panel method)

The hull paneling as shown in Fig. 6 consists of 40×16 in the streamwise and the girthwise directions. The free surface paneling consists of 210×18 in the longitudinal and the transverse directions. The region covered by the free surface panels ranges from -1.0 to 1.2 longitudinally and from the centerline (y=0) or hull surface to 0.7 transversely. When solving a ship wave problem, it should be checked previously that the used grid points on the free surface are enough to resolve the wave pattern. The relevant parameter is the fundamental transverse wavelength ($\lambda_0=2\pi Fn^2$). The usual criterion is that at least 30 points per fundamental wavelength are required. Since the fundamental wavelength is 0.627 at a Froude number of 0.316, the longitudinal grid spacing must be less than 2% of the ship length. The present 210 grid points in the longitudinal direction correspond to 1% of the ship length, which is sufficient for capturing the wave pattern at Fn=0.316.

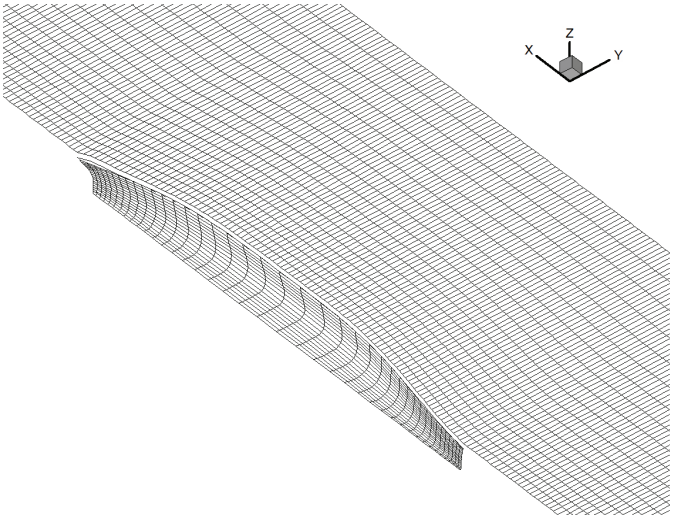

Fig. 6 Panel distribution on the hull and the free surface used in potential method.

Viscous method (finite volume method)

An H-mesh topology is used on the free surface and an O-mesh topology is used in cross sections. The grid consists of 133×57×35 grid points in the streamwise, the girth and the normal directions. The resolution on the hull surface is 82×35. For the viscous method, it is not simple to check the aforementioned criterion for the grid points because the grid spacing is not uniform in longitudinal direction, as shown in Fig. 5. Thus the average grid spacing, when considering the grid points in the longitudinal direction on the hull, is about 1.2% of the ship length. Note that the grid spacing near the midship of a hull is larger than 1.2% due to clustering the grid points to the bow and the stern. But it is supposed that this grid spacing satisfies the criterion. The smaller grid spacing is not used in the present study due to the calculation time of the present viscous method, which takes about 60 *hours* in SGI Onyx2 workstation (R10000 CPU, 344Mflops) for the 133×57×35 grid distribution. On the contrary the potential method takes about 3 *hours* on the same workstation. Thus distributing more grid points is believed to be unpractical as compared with the potential method. The magnified views of the grids near the bow and stern are shown in Fig. 7.

The solution domain is as follows:

$-1.5 \le x \le 2.5 \quad 0 \le y \le 2 \quad -2 \le z \le h(x, y)$ (the wave height)

The wave damping zone illustrated in Fig. 5 is set as follows:

$1.5 \le x \le 2.5 \quad 1 \le y \le 2$

The minimum spacing in normal direction is taken constantly 10^{-3}, which corresponds to 20~100 in y^+. By using the wall function, the minimum spacing in normal direction can be increased and lager than compared to that of near wall turbulence models. The nondimensional time step is taken to be 0.01 and the calculation is made until T=20. The constant acceleration is made in the first 200 steps (T=2).

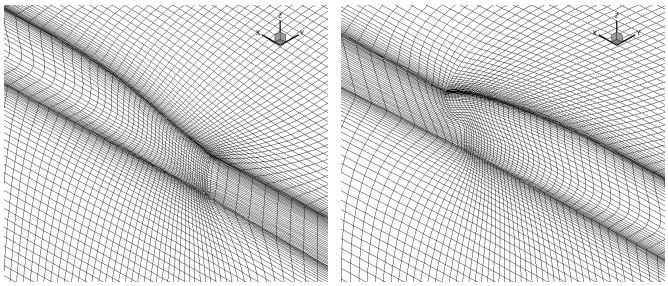

Fig. 7 Grids near a bow and a stern used in viscous method.

Results

The left graph of Fig. 8 shows the wave profile along the hull compared with the experimental data for the panel method, while the right one is the similar comparison for the viscous method. As a whole both calculated results agree well with the experimental data. Especially, the wave profile calculated from the viscous method shows better agreement with the measurement. The only exception is the fullness of the bow wave. This deviation could be due to spray, which is not modeled in the present numerical methods.

On the other hand the wave profile calculated from the potential method shows some deviations com-pared with the viscous result, i.e. the peak values of troughs around x=-0.1, 0.3 are underpredicted. The reason is associated with the generation of a boundary layer and wake near the hull. Another important feature on this underprediction at the troughs is related with the numerical treatments in the present potential method. The collocation points adjacent to the hull are at a rather certain distance from the hull and move up and down only during the nonlinear iterations. Thus the slope of a section shape is not accurately taken into account in the present potential method, with resulting somewhat inaccuracy in the wave profile along the hull. But fortunately this effect is quite localized and has no effect on the general wave pattern. This discussion will be made in the following comparisons of the wave profile along the longitudinal cuts.

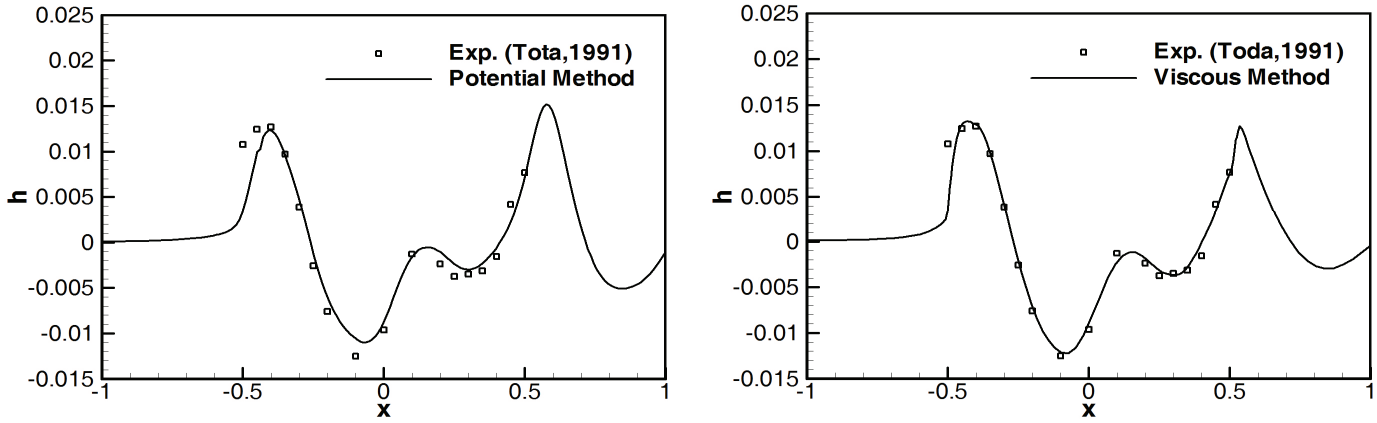

Fig. 8 Comparison of wave profiles along the hull.

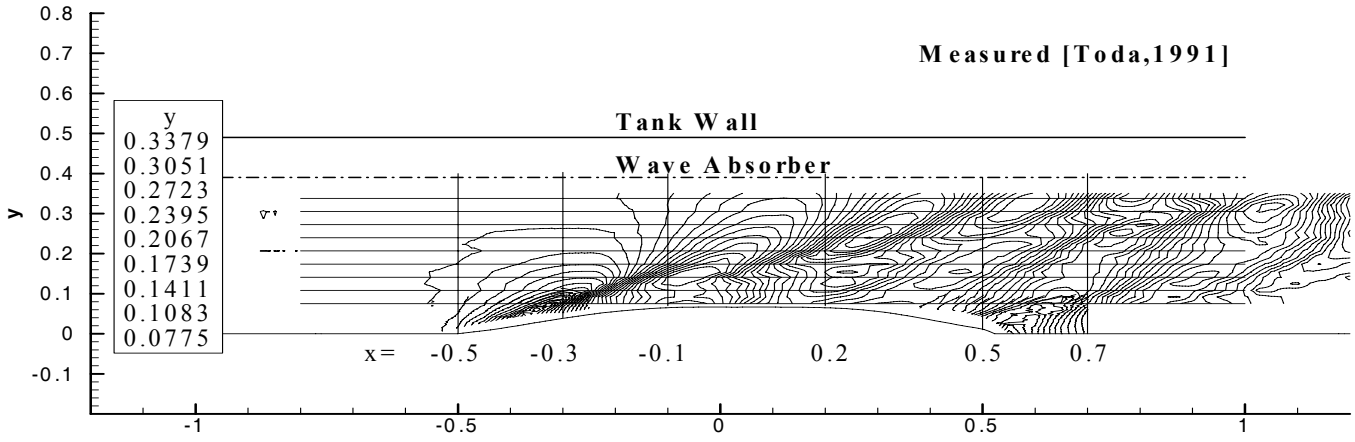

Fig. 9 Positions of longitudinal and transverse cuts.

Fig. 9 provides the overall positions of longitudinal and transverse cuts to be compared in the following discussion. Nine longitudinal cuts for $0.0775 \le y \le 0.3379$ and six transverse cuts for $-0.5 \le x \le 0.7$ are selected for the detailed comparison of the wave patterns by the numerical result and the measurement. As illustrated in Fig. 9, it should be pointed out that the wave absorber and the tank wall are located at y=0.4, 0.5, respectively. Caution is advised in the fact that the y=0.3379 cut is somewhat close to the wave absorber of a towing tank. This discussion will be addressed later.

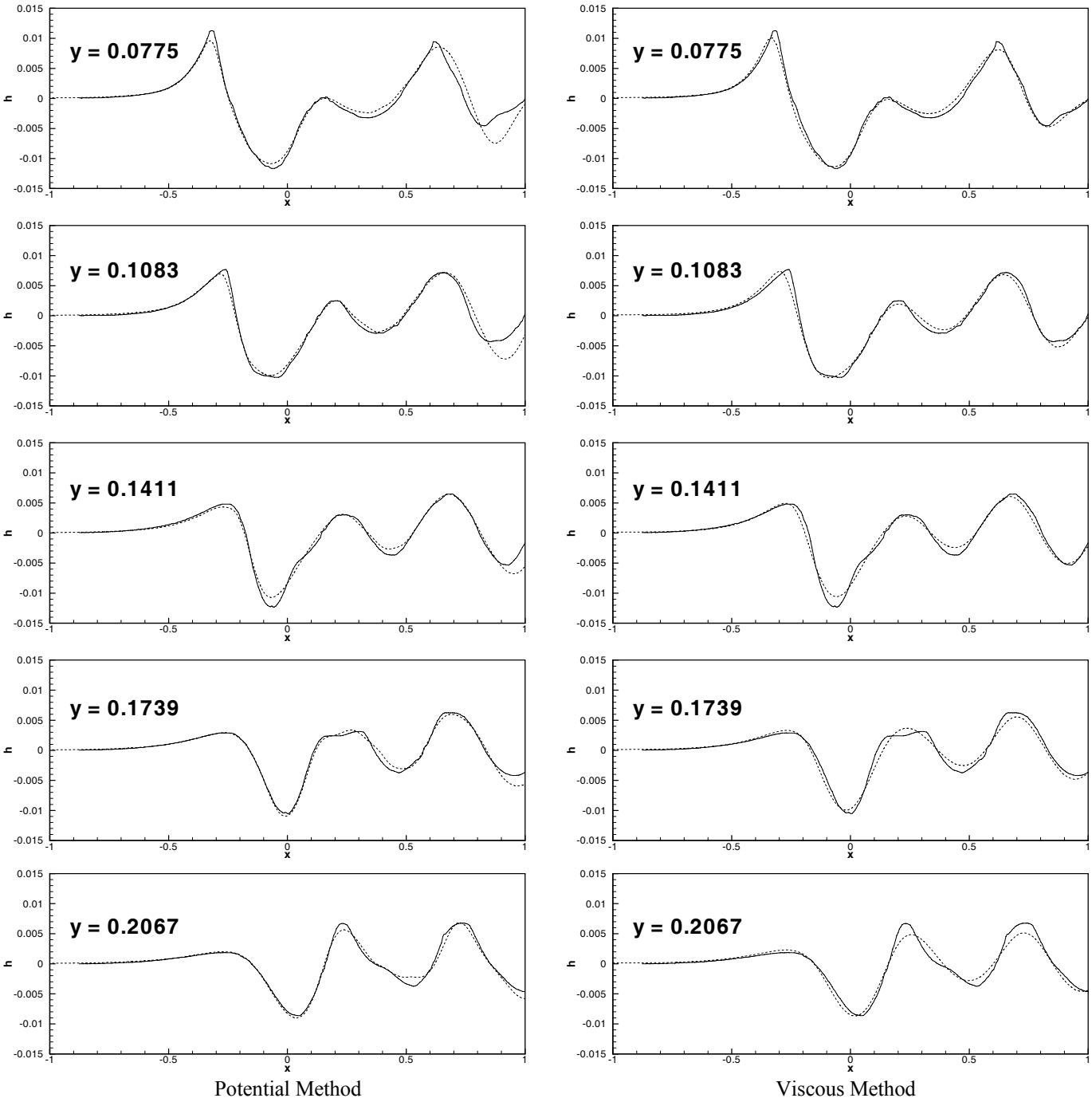

Fig. 10 Comparison of the wave elevations along longitudinal cuts (solid: experiment, dashed: calculation).

Fig. 10 compares calculated and measured longitudinal cuts for the potential method and the viscous method. In these figures the solid line features the measurement and the dotted line features the calculated result. In the first place the overall agreement is excellent in both methods.

First, note that the potential method gives the good agreement with the measurement around x=-0.1 and -0.3 at the y=0.0075 cut in Fig. 10. The inaccuracy of the wave profile shown in Fig. 8 is almost disappeared at the y=0.0075 cut, which is the nearest cut to the hull. The same tendency is also observed at the y=0.1083 cut. From these comparisons it can be deduced that the inaccuracy of the wave profile near the hull surface in the present potential method has no effect on the general wave pattern.

Second, note that in Fig. 10 a large deviation is observed in the amplitude of stern wave system around x=0.9 at the y=0.0075 cut of the potential method. The potential method overpredicts the amplitude of a stern wave. This is caused by viscous effects, which are neglected in the potential method. On the contrary the viscous method predicts very accurately the amplitude of a stern wave at the same cut, which is clearly seen in the viscous result of Fig. 10.

Another interesting feature revealed both by experiment and by computation is that even many of the short-wave features are reproduced by the potential method. Note that in the y=0.1739 cut, the measured data shows the irregular wave form (small hump) around x=0.25, this is due to the presence of a crest of the fore shoulder wave. The potential result in Fig. 10 corresponds quite well to this short length wave with correct phase and position. In the viscous result, however, this wave does not appear because of the numerical dissipation of the viscous method.

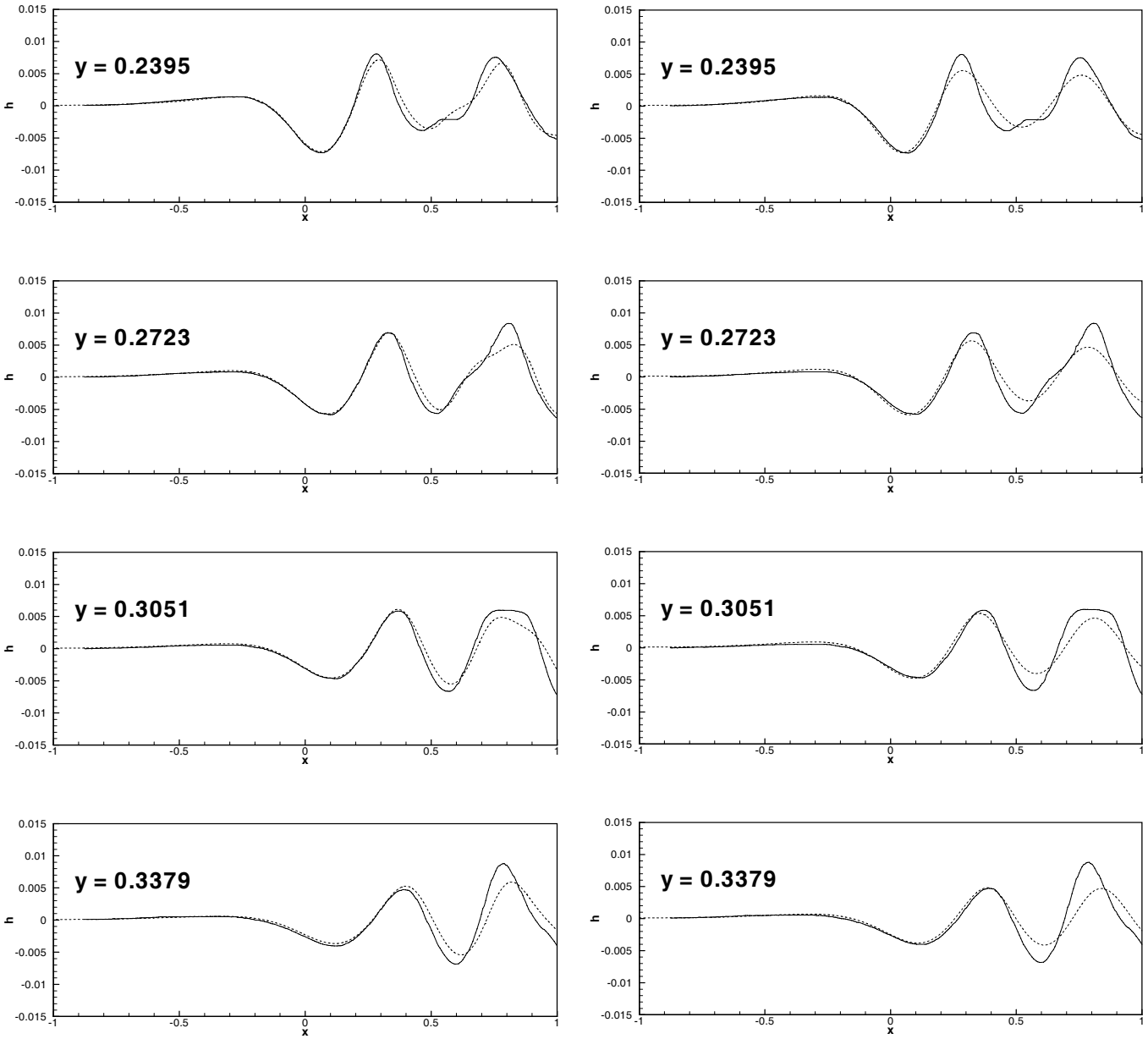

Fig. 11 Comparison of the wave elevations along outer longitudinal cuts (solid: experiment, dashed: calculation).

Fig. 11 shows the similar comparisons of the calculation and the experiment for somewhat outer longi-tudinal cuts for the potential and viscous methods. It is observed that at the outer longitudinal cuts the agreement is not as good as the previous inner longitudinal cuts in Fig. 10. The numerical damping now actually enters (most clearly at the y=0.3379 cut) in the potential method. This numerical damping is observed more obviously from the comparison between the viscous calculation and the experiment in Fig. 11. It is particularly interesting to observe that the downstream part of the outer cuts contains some phase deviations especially at the y=0.3379 cut. But a closer inspection shows that these phase deviations in the experiments move forward rather than aft when going further away from the hull (see y=0.3051,3379 cuts). As previously mentioned, the wave measurements at y=0.3051, 3379 cuts may be somewhat affected by the partial wave reflections at the wave absorber located at y=0.4.

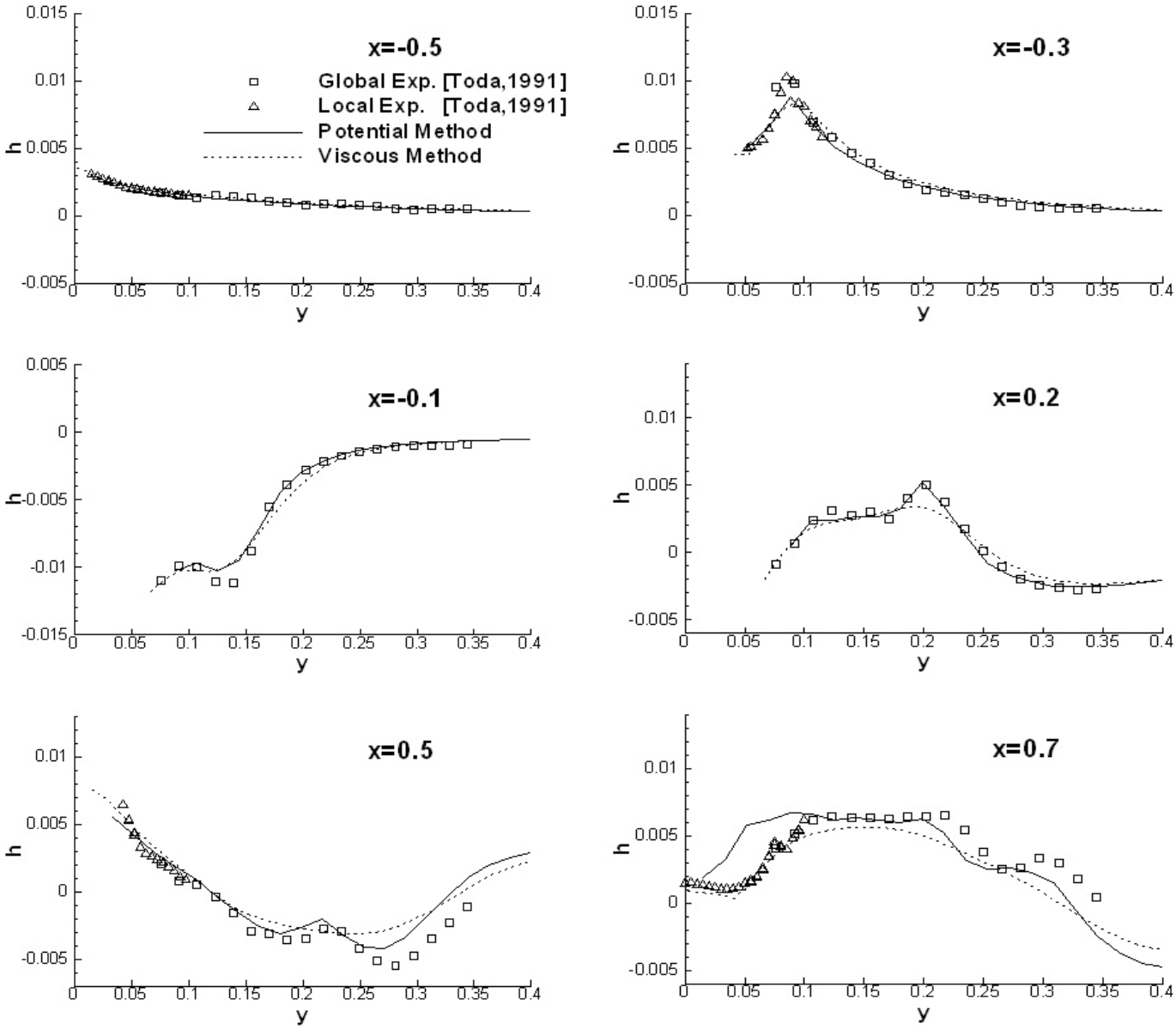

Fig. 12 Comparison of the wave elevations along transverse cuts.

Fig. 12 shows the comparisons of the transverse wave cuts at the various x-positions. In the x=0.2 sec-tion, the viscous method in contrast with the potential method fails to predict the small wave hump lo-cated around y=0.2, which corresponds to the shoulder wave. The similar tendency can be seen in the x=0.5 section. These two comparisons of transverse wave cuts clearly indicate that the numerical dissipa-tion of the viscous method is excessively higher than that of the potential method in the present grid dis-tributions. These indications were not clearly visible in the comparisons of the longitudinal cuts.

The comparison of the transverse wave cut at the x=0.7, which is located in the wake region of a ship, reveals the whole situations of the potential and viscous methods. The viscous method gives fairly good agreements with the measurement in the highly viscous region such as the region up to y=0.1. On the con-trary the potential method simulates poorly the stern wave at that region. But in the outer inviscid region (greater than y=0.1), the potential result is much better than the viscous result, i.e., the flat stern wave from y=0.1 to y=0.2 is well predicted and the peak of a transverse wave is more clearly captured. Fig. 13 and Fig. 14 show the comparison of wave contours compared with the measurements for the potential and viscous methods, respectively. Two computational results simulate the bow wave and the first trough fairly well. The differences are apparent in the region away from the hull. The diverging waves in the viscous method look too smooth compared with the experiment and the potential result.

These results are considered to be due to smaller numerical damping in the potential method. Since the present potential method is one of boundary element methods, a governing equation, i.e. Laplace equation, is already satisfied by the distributed source panels. And also the body boundary condition, which states that the normal velocity must be zero on the hull, does not require any discretization procedures.

Thus the main numerical damping enters only when the combined free surface condition is discretized in the present potential method. But the viscous method requires the discretization procedures of both the governing equations in the whole computational domain and the boundary conditions including the free surface conditions. Accordingly the viscous method has inherently more numerical damping than the potential method. This result clearly indicates that the viscous method needs more grid points on the free surface compared with the potential method.

A closer examination of the wave pattern right behind a stern in Fig. 13 and Fig. 14 shows that the viscous method is superior to the potential method in the wake region. This feature is immediately ob-vious from the Fig. 15, which shows the magnified view of the wave pattern and the velocity vectors in the wake region of a ship. The velocity vectors in the viscous method show clearly the presence of the thickened boundary layer near a stern. The large velocity vectors from the potential method make the wave pattern behind a stern overpredicted compared with the viscous method (see Fig. 10).

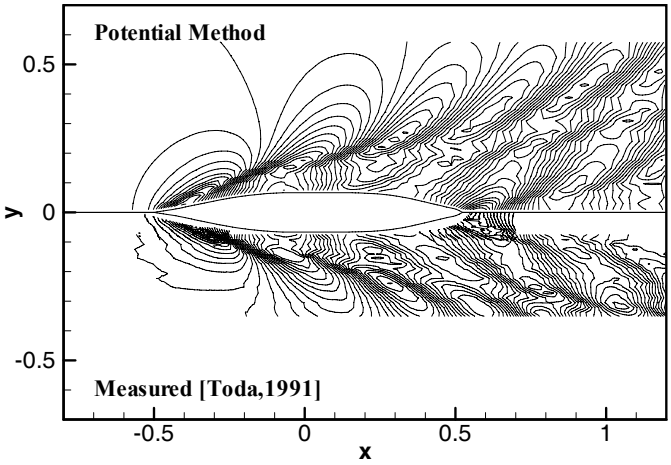

Fig. 13 Wave patterns from the potential method and the measurements.

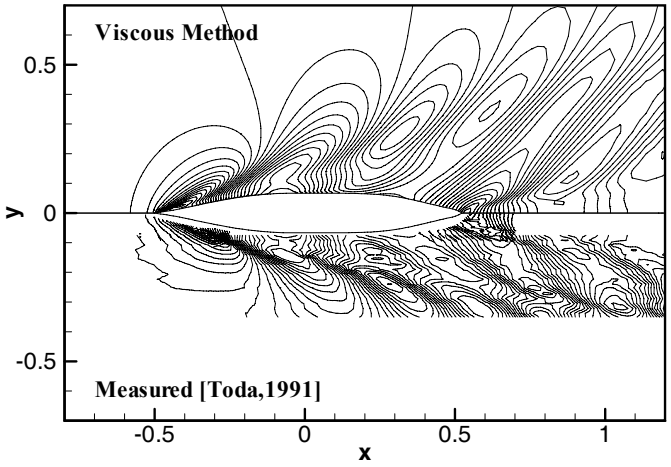

Fig. 14 Wave patterns from the viscous method and the measurements.

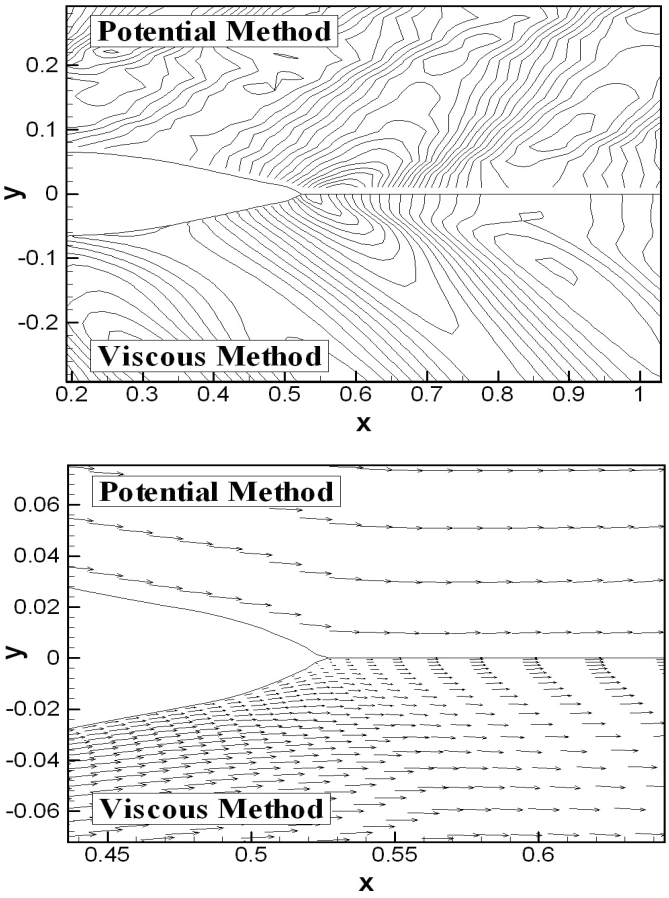

Fig. 15 Close up view of the region near a stern.

CONCLUSIONS

The recent state-of-the art potential and viscous methods are used to solve the nonlinear ship wave problem, based on the panel method and the finite volume method, respectively. The extensive comparisons with the wave measurements of Series 60 hull are performed with the numerical results from both methods in order to evaluate the capability of predicting the ship wave pattern. Generally, both methods show good agreements with the wave measurements. But closer inspections reveal the advantages and disadvantages of both methods for predicting the ship wave patterns. The potential method is sufficiently accurate for the global wave patterns (e.g. the diverging waves) except the region near a stern. On the contrary the viscous method shows remarkable similarity to the wave in local region near the hull, but the global wave pattern away from the hull is not captured accurately.

Up to now the potential method is a very useful tool for solving the nonlinear ship wave problem because of its numerical robustness and computational efficiency. But the ultimate goal is the viscous method taking into account a free surface. If further researches are performed on the damping-free schemes and the algorithm for fast calculation, the viscous method can be a useful design tool for ships in the near future.

ACKNOWLEDGEMENTS

This research was supported by MOERI/KORDI basic research grant PES141B and PKS0500 under the administration of Korea Research Council of fundamental Science and Technology and also sponsored by research grant PNS1740 under the administration of the ministry of knowledge economy, Korea government.

REFERENCES

Beddhu, M. Jiang, M.Y. Taylor, L.K. and Whitfield, D.L., 1998. Computation of steady and unsteady flows with a free Surface around the Wigley hull. *Applied Mathematics and Computation*, 89, pp.67-84.

Farmer, J. Martinelli, L. and Jameson, A., 1994. Multigrid solutions of the Euler and Navier-Stokes equations for a Series 60 Cb=0.6 ship hull for Froude numbers 0, 0.160, 0.220, 0.316. *Proc. of CFD Workshop*. Tokyo, Japan.

Ferziger, J.H. and Peric, M., 1996. *Computational Methods for Fluid Dynamics*. Springer-Verlag. Berlin.

Hinatsu, M., 1992. Numerical simulation of unsteady viscous nonlinear waves using moving grid system fitted on a free surface. *J. Kansai Soc. Naval Arch*, 217, pp. 1-11.

Hino, T., 1994. A study of grid dependence in Navier-Stokes solutions for free surface flows around a ship hull. *Journal of the Society Naval Architects of Japan*, 176, pp.11-18.

Janson, C.E., 1997. *Potential flow panel methods for the calculations of free-surface flows with lift*. Ph.D. Thesis. Gothenburg: Chalmers University.

Khosla, P.K. and Rubin, S.G., 1974. A diagonally dominant second-order accurate implicit scheme. *Computers and Fluids*, 2(2), pp.207-209.

Kim, D.H. Kim, W.J. Van, S.H. and Kim, H., 1998. Nonlinear potential flow calculation for the wave pattern of practical hull forms. *3th Int. Conf. on Hydrodynamics*. Seoul, Korea.

Kim, J.J. Kim, H.T. and Van, S.H., 1998. RANS simulation of viscous flow and surface wave fields around ship models. *Proc. of the third Osaka Colloquium on Advanced CFD Applications to Ship Flow and Hull Form Design*. Osaka, Japan.

Kim, W.J. Kim, D.H. and Van, S.H., 1999. Calculation of turbulent flows around VLCC hull forms with stern frameline modification. *7th Int. Conf. Numerical Ship Hydrodynamics*. Nantes, France.

Kodama, Y., 1994. An International Workshop for Improvement of Hull Form Designs. *Proc. of CFD Workshop Tokyo*. Tokyo, Japan.

Miyata, H. Sato, T. and Baba, T., 1987. Difference solution of a viscous flow with free-surface wave about an advancing ship. *Journal of Computational Physics*, 72, pp.393-421.

Muzaferija, S. and Peric, M., 1997. Computation of free surface flows using finite volume method and moving grids. *Numer. Heat Transfer*, Part B, 32, pp.369-384.

Raven, H.C., 1988. Variations on a theme by Dawson. *17th Symposium on Naval Hydrodynamics*. Hague, The Netherlands.

Raven, H.C., 1996. *A solution method for the nonlinear ship wave resistance problem*. Ph.D. Thesis. Delft University of Technology. Hague, The Netherlands.

Rhie, C.M. and Chow, W.L., 1983. Numerical study of the turbulent flow past an aerofoil with trailing edge separation. *AIAA J*, 21(11), pp.1525-1532.

Schumann, C., 1998. Computing free surface ship flows with a volume-of-fluid method. *7th Int. Symposium on Practical Design of Ships and Mobile Units*. Hague, The Netherlands.

Söding, H., 1994. Incomplete Gauss elimination. *Ship Technology Research*. 41(2), pp.111-112.

Stone, H.L., 1968. Iterative solution of implicit approximations of multi-dimensional partial differential equations. *SIAM J. Numer. Anal*, 5(3), pp.530-558.

Toda, Y. Stern, F. and Longo, J., 1991. Mean flow measurements in the boundary layer and wake field of a Series 60, CB = 0.6 ship model for Froude number 0.16 and 0.316. *IIHR Report No. 352*. Iowa, USA.